Soft Origami Gripper with Variable Effective Length

*Bohan Chen, Zhuyin Shao, Zhexin Xie, Jiaqi Liu, Fei Pan, Liwen He, Li Zhang, Yanming Zhang, Xuechen Ling, Fujun Peng, Weidong Yun, and Li Wen**

Nature has evolved to shape morphing to adapt to complex environments while engaging with the surroundings. Inspired by this capability, robots are expected to be endowed with the ability to perform shape-changing, thus interacting with complex environments. Herein, a soft origami actuator with variable effective length (VEL) is proposed to adapt to different objects. The actuator's VEL is realized by an origami structure and actuated by hybrid actuation of tendons and pneumatic pressure. The soft actuator yields motion combining both elongation and bending generated by the asymmetric Yorshimura origami structure. Then an adaptive gripper composed of four origami actuators with programmable effective length is fabricated and its effect on grasping performance is evaluated through both simulations and experiments. Results show that the gripper can grip objects of different shapes, weights, sizes, and textures. This research may shed light on a new soft gripper design using origami structure for the environment's self-adaptability.

1. Introduction

Soft-bodied animals such as leech have attracted great interest from researchers because their ductile skins are full of special annular folded structure.[1,2] They yield not only a strong ability to resist mechanical load, but also superior body which can extend the capability to realize effective motion of moving, adhesion, and grasping in complex environments.[3] Inspired by these features, soft robotics have endowed locomotion such as crawling,[4] obstacle avoiding, and grasping in restrictive environments.[5,6] As the size and shape of the gripped targets are uncertain, the variable effective length (VEL) grasping soft robot is a promising solution for these types of issue.[7] However, the existing gripper with VEL is achieved by limiting the bendable part of the actuator without length changing, which greatly limits the grasp range.

Adaptable and effective grasping has attracted growing attentions in the field of soft robotics recently. Using the structural design to achieve effective grasping has become a popular approach.[8–10] A universal gripper based on soft material actuation has various applications for gripping objects of different sizes and shapes. Nevertheless, we need a scalable structure to enlarge the grasping space further. The origami structures have this potential.[11,12] Recent works have not yet considered VEL by investigating the origami structure's kinematic model. But it is unclear that how can geometrical parameters of origami affect the soft actuator's elongation. Furthermore, how to decouple the elongation and bending motion through hybrid actuation, i.e., the pneumatic and cable-driven, needs to be addressed.

Origami has been applied in soft robotics with many successful examples, such as crawling robot,[13] surgical robot, and soft arm.[14,15] However, recent works rarely focus on the geometrical parameter analysis, kinematic model, and VEL. How does geometrical parameter impact actuator motion trajectory? How to use the elongation property of origami structure in grasping and decouple the elongation and bending motion? Can the VEL influence the gripping performance of the soft origami gripper?

There are few studies on programmable effective length soft grippers for different size targets. In this study, we developed a bioinspired asymmetric Yoshimura origami folding structure to achieve both elongating and bending motion. The Yoshimura origami structure enables one side of the actuator's length to be easily controlled via cables. Then we applied pneumatic-cable hybrid actuation to realize the length of the actuator's inner side to be controllable. We introduced design and fabrication details of the origami unit cells and the whole actuator, explored the origami device's structural parameters, and then fabricated a scalable soft gripper. Finally, simulation and experiments were conducted to examine the effect of different effective lengths on grasping objects of different shapes, weights, sizes, and textures.

Dr. B. Chen, Z. Shao, Dr. Z. Xie, J. Liu, Dr. F. Pan, L. He, Y. Zhang, X. Ling, Prof. L. Wen
School of Mechanical Engineering and Automation
Beihang University
Beijing 100191, China
E-mail: liwen@buaa.edu.cn

L. Zhang
School of Automation Science and Electrical Engineering
Beihang University
Beijing 100191, China

Dr. F. Peng, W. Yun
Shanghai Institute of Aerospace System Engineering
Shanghai 201108, China

(iD) The ORCID identification number(s) for the author(s) of this article can be found under https://doi.org/10.1002/aisy.202000251.

2. Experimental Section

Leech can still move effectively with its unique movement pattern on complex surfaces. The characteristic of the special movement is coupled with elongation and bending. **Figure 1**b shows that the elongation of the body is characterized by two functional different modes of morphing: elongation and bending. A leech can move the distal end of its body to the next position by stretching body to 2–3 times the body length and bend its body to attach to the surface via the distal end. Elongation and bending are often coupled motions. This embodied extreme morphing is attributed to the coexistence of folded hierarchical geometry and stretchable skin of leech's skin structure. Inspired by this elongating–bending movement pattern, we proposed an improved Yoshimura origami structure with similar motion capability (Figure 1a).

The difference between the improved Yoshimura origami structure and the traditional structure lies in the unit cell of the origami structure (Figure 1c,d). By controlling the apex angles β_1 and β_2 of the expanded structure (Figure 1d), the Yoshimura origami structure not only has larger elongation but also produces directional bending motion due to the different elongation rates between dorsal and ventral sides. To verify the improved Yoshimura origami, we constructed an artificial structure that mimics the stretching, bending, and adsorption processes of leeches as they moved forward (Figure 1b).

In this study, we focused on elongating and bending coupled motion of the soft robot: first, we numerically studied the impact of the Yoshimura origami structure parameters on elongating–bending motion, as well as its application in artificial system control method, and then applied the results to guide the scalable gripper design on improving the grasping motion.

### 2.1. Geometry Analysis of a Soft Origami Actuator

The crease structure of a single actuator was inspired by the Yoshimura origami structure and modified to meet the need for elongating and bending (Figure 1c). The top and side views of the repeated origami unit of the origami structure are shown in Figure 1c. Repeated origami unit consist of three-unit cells. Red and green lines represent the lateral side and ventral side of the actuator, respectively. The expansion structure consists of three-unit cells that will be folded, respectively, framed in red, green, and orange squares (Figure 1d).

Figure 2a shows the partly folded configuration. Angle β between the mountain fold line and the valley fold line is defined as the apex angle of the unit cell. Angle θ is defined as the fold angle between the rigid plate with shade lines and the vertical plane of the unit in Figure 2a; θ is 0° in the fully foldable state and 90° in the fully unfolded state. The apex angle β of the unit is constant during the deployment of the origami, but its projections on the horizontal and vertical planes are changing.

The projections of the apex angle β on the horizontal and vertical planes during the motion are shown in Figure 2b. The
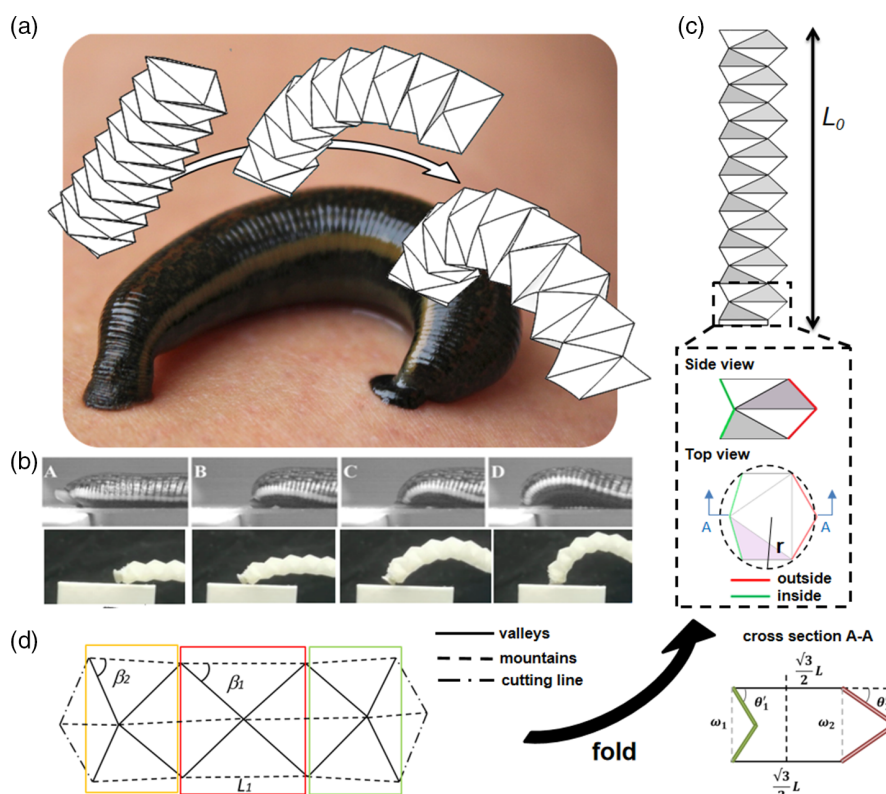
Figure 1. Leech-inspired asymmetric Yoshimura origami structure. a) Asymmetric origami actuators inspired by leech movement patterns. b) The movement process of leech and corresponded movement process of soft origami actuator integrated with a sucker. c) Side/top views of the origami actuator unit cell. d) Top view of the fully unfolded origami structure (red, orange, and green box represents three unit of the origami structure).
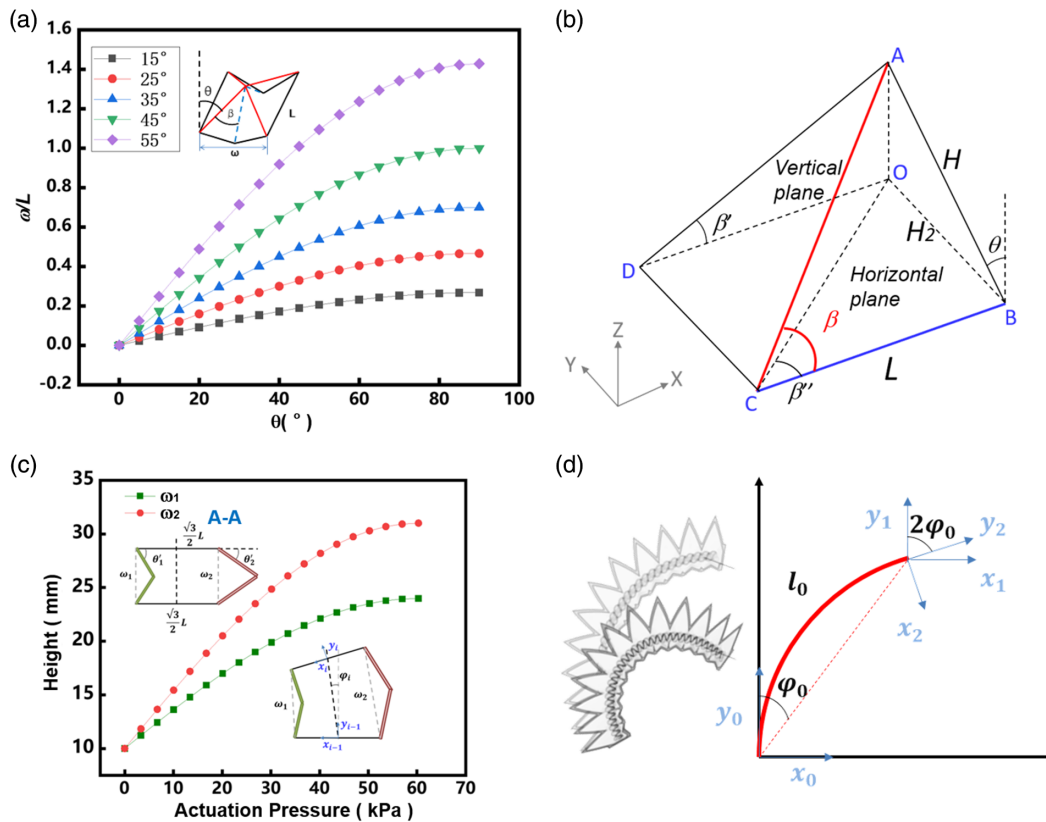
Figure 2. Parametric study of asymmetric Yoshimura origami unit. a) Longitudinal length ω/L as a function of defining angle θ under different apex angles β. The inset image shows the unit of origami, with six creases definition of parameters longitudinal length ω/L, angle θ, and apex angles β are given. b) Projection of the apex angle. c) Inner longitudinal directions (ω_1) and outer longitudinal directions (ω_2) of the origami unit cell as a function of air pressure diagram. The inset image is the cross section of an origami repeated origami unit. d) The mathematical model to describe the variable DOF of the actuator.

projection of the apex angle β on the vertical plane is β' and on the horizontal plane is β''; L is the length of the basic triangle plate.

In the right triangles $\triangle ABC$, $\triangle OAB$, and $\triangle OBC$ of Figure 2b, we have

$$H = L \tan \beta \tag{1}$$

$$H_2 = H \sin \theta \tag{2}$$

and

$$H_2 = L \tan \beta'' \tag{3}$$

Substituting Equation (1) and (2) into Equation (3), we can calculate the projection of apex angle β on the vertical plane

$$\tan \beta'' = \tan \beta \sin \theta \tag{4}$$

The width of the basic units along the longitudinal length ω is

$$\omega = L \tan \beta'' = L \tan \beta \sin \theta \tag{5}$$

According to Equation (5), the apex angle β depends on the longitudinal length ω. To reduce the influence of origami unit

size on longitudinal length, we explore the relationship between the apex angle β and a relative longitudinal length ω/L. As shown in Figure 2a, the trends of all curves are similar. The relative longitudinal length ω/L increases continuously with the increase in the fold angle θ. The relative longitudinal lengths of all models are 0 in the fully folded state and equal to $\tan\beta$ in the fully deployable state. We elaborated the rigid-foldability of the origami structure, as shown in Figure S1 and S2, Supporting Information.

As shown in Figure 2c, we set the apex angle β of the inner and outer origami units at 25° and 35°, respectively. The projection of the inner and outer origami units' fold angle θ onto cross-section A-A are θ_1' and θ_2'; their relationship is shown in Equation (6). The figure shows the change curve of the inner and outer longitudinal directions (ω_1 and ω_2) with air pressure.

$$\begin{aligned} {}^i_0T &= {}^1_0T \cdot {}^2_1T \ldots {}^i_{i-1}T \\ &\left(\frac{\pi}{2} > \theta > 0, \ \frac{\pi}{2} > \beta > 0\right) \end{aligned} \tag{6}$$

As the actuator is made up of several origami units in series, we made the following assumption[16]:

1) Origami units have constant curvatures. 2) The curves are tangent at the intersection points.

The forward kinematics solve the transformation from side length $\{\omega_1, \omega_2\}$ (joint space) to end effector coordinates $\{x, y\}$ (task space) according to Equation (11). Equation (7)–(10) show the modeling of a single segment.

$$\varphi_i = \arcsin \frac{\omega_2 - \omega_1}{\sqrt{3}L} \tag{7}$$

$$_{i-1}^{i}T = \begin{bmatrix} R_i & P_i \\ 0 & 1 \end{bmatrix}_{4\times4} \tag{8}$$

$$R_i = \begin{bmatrix} \cos 2\varphi_i & \sin 2\varphi_i \\ -\sin 2\varphi_i & \cos 2\varphi_i \end{bmatrix} \tag{9}$$

$$P_i = \begin{bmatrix} \frac{(\omega_1+\omega_2)\sin\varphi_i}{2} \\ \frac{(\omega_1+\omega_2)\cos\varphi_i}{2} \\ 0 \end{bmatrix} \tag{10}$$

$$\theta' = \arccos \frac{\cos\theta}{\sin\beta\tan\beta} \tag{11}$$

Through geometric analysis, it is known that apex angle β is the main factor that affects the elongation rate of origami units. By controlling the value of β on both sides of the origami actuator, the actuator can bend in the specified direction.

A mathematical model was established to describe the kinematics of the actuator under the various motion patterns. We hypothesize that the boundaries between the neighboring sections are tangent and focused on the bottom profile of the actuator. As Figure 2d shows, the bending of one section could be represented by translating the coordinate X_0–Y_0 to X_1–Y_1 with the distance d, and then rotating with the angle $-2\varphi_0$ to X_2–Y_2. φ_0 is superposed by the rotation angles of i origami units and the relationship is shown in Equation (12). So, the homogeneous transformation matrix from X_0–Y_0 to X_2–Y_2 is shown in Equation (13).

$$\varphi_0 = \varphi_1 + \varphi_2 + \ldots\ldots + \varphi_i \tag{12}$$

$$_{0}^{2}A = \begin{bmatrix} \cos 2\varphi_i & \sin 2\varphi_i & 0 & \frac{(i\cdot\omega_1+i\cdot\omega_2)\sin\varphi_i}{2} \\ -\sin 2\varphi_i & \cos 2\varphi_i & 0 & \frac{(i\cdot\omega_1+i\cdot\omega_2)\cos\varphi_i}{2} \\ 0 & 0 & 1 & 0 \\ 0 & 0 & 0 & 1 \end{bmatrix} \tag{13}$$

where l is the length of the actuator. When the cable of length l_0 limits the length of actuator inner side (the effective length of the actuator), Equation (13) could be rewritten as

$$_{0}^{2}A = \begin{bmatrix} \cos 2\varphi_i & \sin 2\varphi_i & 0 & \frac{(l_0+i\cdot\omega_2)\sin\varphi_i}{2} \\ -\sin 2\varphi_i & \cos 2\varphi_i & 0 & \frac{(l_0+i\cdot\omega_2)\cos\varphi_i}{2} \\ 0 & 0 & 1 & 0 \\ 0 & 0 & 0 & 1 \end{bmatrix} \tag{14}$$

According to this mathematical model, for each bending degree of freedom (DOF), one can obtain the profile of the actuator with the curvature as the input. We first changed the cable length of the actuator based on the geometric features of the objects, and then inflated the actuator to achieve more stable and active-adaptable grasping.

2.2. Materials and Manufacturing

In the previous part, the geometric shape design of the soft origami actuator was introduced in detail. Considering the stiffness of leech skin, we chose Mold Star 30 to fabricate the actuators. The details of the soft origami actuators were used in the finite element (FE) simulations. The influence of fiber length on actuator's trajectory is verified by experiment (**Figure 3**a). We have done a series of experiments and simulations to explore the effect of geometric design parameters and cable-driven actuation on shape-controllable (Figure S3–S5, Supporting Information). The lost wax casting process was used to manufacture a complex inner cavity; the wax was used to fabricate the inner mold and then it was heated to melt to form the cavity (Figure 3c); and finally, four actuators were attached with fibers and composed into a whole gripper (Figure 3b).

2.3. Grasping Simulations

After characterizing the functional characteristics and decoupling control mode of the soft origami actuator, the scalable gripper consisted of soft origami actuators has ability to grasp objects. We explored the practical application of the scalable gripper. The scalable gripper has the features of lightweight, high expansion ratio, and VEL; these features provide it with great advantage in space and underwater applications such as in space debris capture missions, microgravity capture, multisize range of objects, and high transportation costs. The requirements for stable grasping process including large workspace, passive compliance, lightweight, and foldability promote the development of gripper.

However, the soft gripper which requires force sensors or strain sensors and a central processor to make decisions can achieve adaptive grasping.[17–20] Due to the high transportation costs and extremely harsh conditions in space tasks, a simplified control system is necessary. The soft material and origami structure of the scalable gripper make it soft, light, compliant, and foldable, and these features are suitable for space tasks. We explored the capture effect of the gripper in the microgravity environment using kinematic simulation. To reduce variables, we simplified the capture task to grasp a relatively static target at an appropriate effective length under a weightlessness simulation environment (**Figure 4**b).

2.3.1. Simulation of Single Actuator

First, the static simulation of a single actuator contacting an object is conducted. To reduce the calculation complexity and shorten the calculation time, several simplifications are made. We considered the actuation process as a quasi-static process, and use the static analysis to study the contact statue of the actuator. The object to be contacted is set as a rigid body.

As shown in Figure 4a, the states of a single finger ($L = 35$ mm, $L_0 = 150$ mm, $\beta_1 = 25°$, $\beta_2 = 35°$, $i = 30$) at the initial state when pressure $= 0$ kPa and at the actuated state when pressure $= 81$ kPa are given. From the results shown in Figure 4a, it can be seen that the soft actuator yielded obvious bending during the actuation.
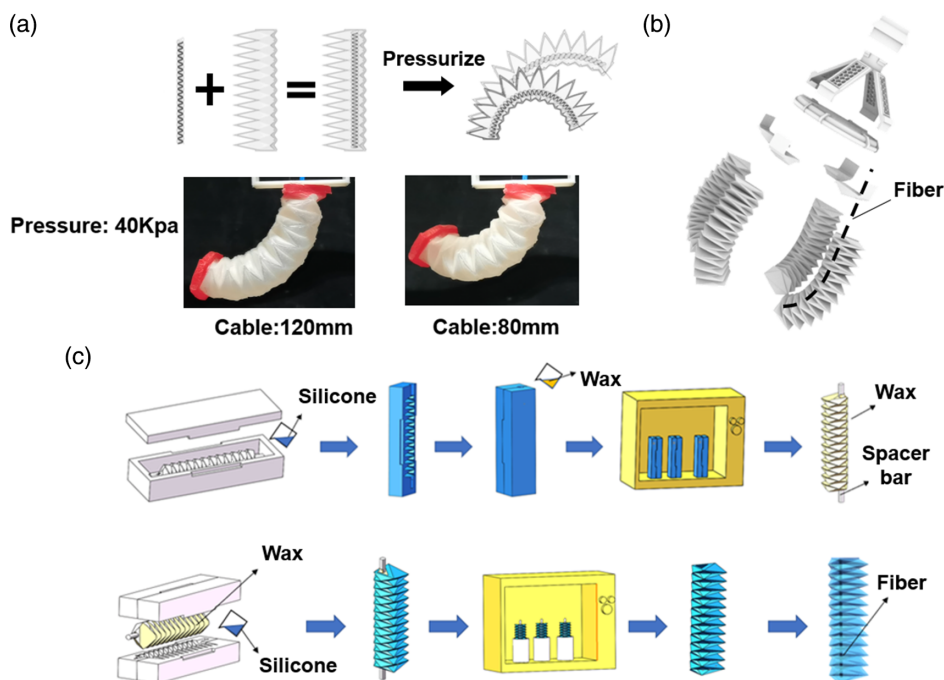
Figure 3. Soft gripper consisting of origami actuator and fiber. a) Prototype of actuator with the same air pressure at 120 mm cable and 80 mm cable. b) The scalable gripper. c) Lost wax casting process.

2.3.2. Simulation in Microgravity Environment

It is considered that we should use the simplest possible control system for space tasks, and then we used the same strategy to grasp objects with different size, shape, and orientations in FE simulation.

As the shape and attitude of space debris are uncertain, we selected several representative cases for simulation to verify the property that if the gripper can still maintain closed force under these cases.[21] We simulated three typical spatial target structures (cylinder, cube, and slab) and three grasping orientations (plane, angle, and edge), and the same spatial target structure was captured from different orientations (Figure 4c). In the simulation experiment, two pairs of actuators with opposite positions are used to capture objects, as shown in Figure 4b. We set the length of the finger as 150 mm and the size of the cylindrical object as $\Phi100 \times 100$ mm. Grab direction refers to the projection of the gripper center on the object. Figure 4b shows the grasping orientation "edge." First, the application view of the scalable grip on the cylinder is designed, and the cylinder is captured when it is oriented in axial, radial, and diagonal directions. The VEL of the gripper is 150 mm and the maximum side length of the objects is 100 mm. The inflating pressure for all the cases is 80 kPa. From the simulation results, it can be seen that two actuators have a good clawing effect and play a major role in grasping. The attached place with objects is mainly in the middle and front end of actuators. The other two actuators were in poor adhesion condition, mainly at the base and the tip of the fingers.

The aforementioned seven simulation situations that the prototype can grasp different objects and the simulated results of contact area and contact stress indicate that the grasping of these objects is stable and valid.

The average contact stress results are shown in Figure 4d. It can be seen from the figure that the gripper in the microgravity environment can adapt to most objects because of its controllable motion process and great passive compliance. Combining adhesion techniques, the origami gripper may have tremendous object capture capability outside of space.[22]

3. Results

The modified Yoshimura origami structure could achieve the coupling of elongating and bending, which guided the design of the soft gripper to realize the passive and compliant grasping motion. Combined with an inextensible cable, the soft asymmetric Yoshimura origami actuator was capable of multiple gripping motions through programmable effective length.

The unique coexistence of flexibility and rigidity of origami structure can be better applied to problems that are difficult to be solved by traditional soft gripper with constant length,[23] such as 1) dynamically changed environments, 2) confined space, and 3) tasks involving interaction with humans or fragile objects.[6]

However, previous efforts were focused on elongating origami actuators and bending origami actuators;[24,25] little research has been done on coupled stretching and bending motion with programmable effective length.

3.1. Mechanical Properties of the Actuator

Before we characterize the scalable gripper, we first characterize the actuators separately to understand the workspace, intensity, and operating pressure.[26] These measurements are then used to guide the gripping and manipulation of the scalable gripper.

2000251 (5 of 9)
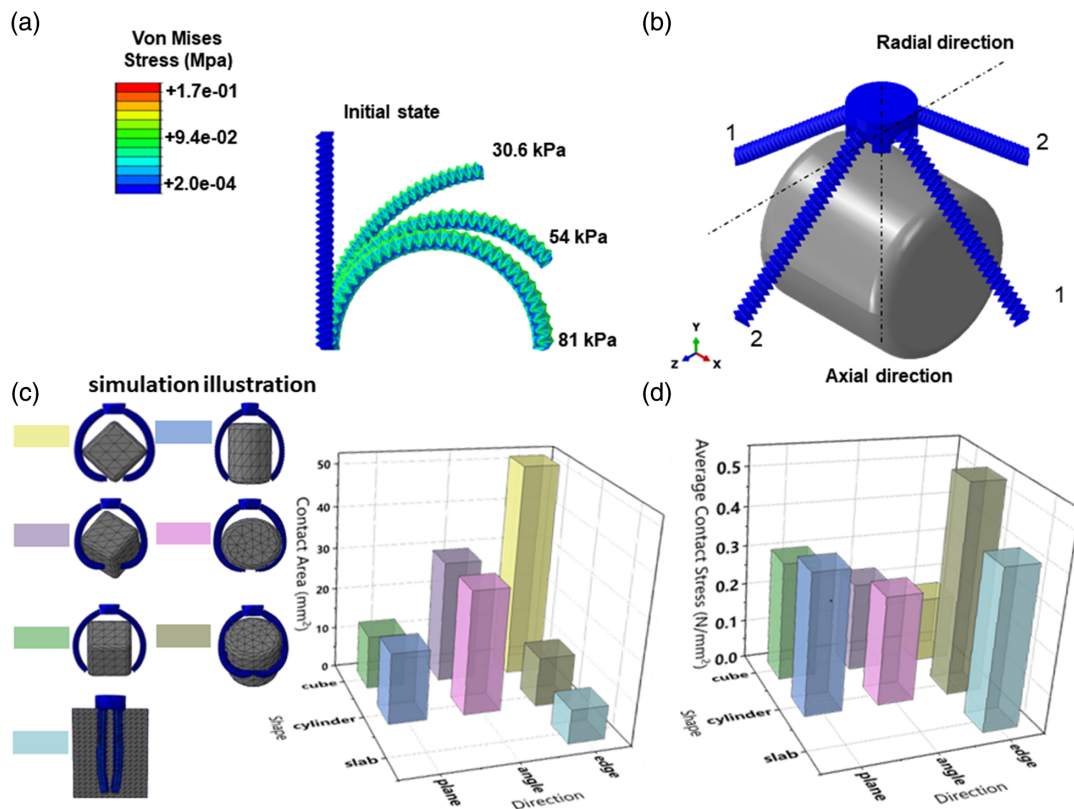
Figure 4. Capture simulation in the microgravity environment. a) The states of a single finger at the initial time and at the last time. b) Cylinder grab simulation. c) In the microgravity environment, the contact area of grasping simulation is a function of the structure of the objects (cylinders target, cube target, and slab target) and the direction of the grasping (plane, angle, and edge). The VEL of the gripper is 150 mm and the maximum side length of the objects is 100 mm. The inflating pressure for all the cases is 80 kPa. d) The average contact stress results when the scalable gripper grips a variety of objects using different grasping direction.

To measure the bending curvature of the actuator ($L = 10$ mm, $L_0 = 80$ mm, $\beta_1 = 25°$, $\beta_2 = 35°$, $i = 8$) along the main grasping axis, we applied to control pressure from 0 to 60 kPa to the inner cavity of the actuator, and measured the three-point displacement along the length of the actuator when the length of the actuator was limited to 80 mm by the cable. Then, the bending curvature of the actuator is calculated from the marked position using the least square fitting circle. The results are shown in **Figure 5**a. The bending curvature k increases nonlinearly with pressure as the function shown in Equation (15).

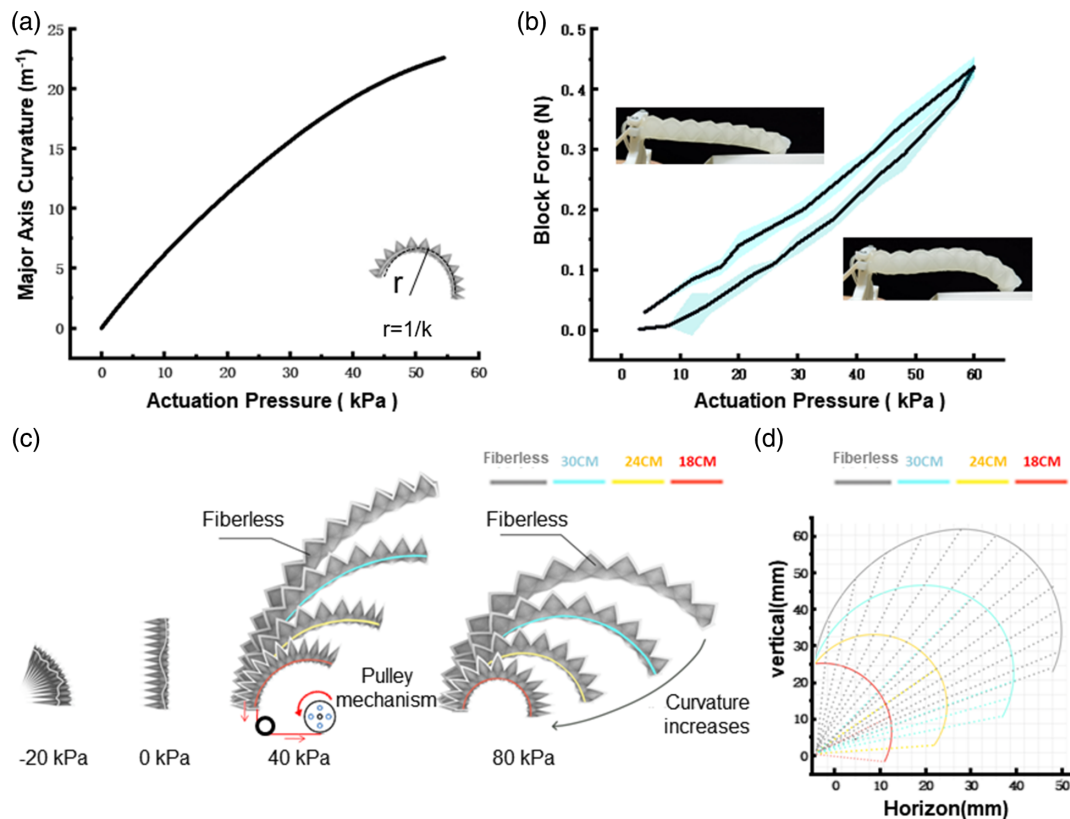$$k = 0.069 + 0.647p - 0.004p^2 \tag{15}$$

To evaluate the strength of soft origami actuators, we measured the blocked force during actuation. A force sensor was mounted under the actuator as shown in Figure 5b; the finger was inflated from 0 to 60 kPa; and the vertical blocking force was measured. The test was repeated 3 times and the blocking force at the pressure of 60 kPa was about 0.45 N.

To adapt to more complex working conditions, the elongation and bending motion of the soft origami actuator is needed to be decoupled. An inextensible cable made of nylon fiber is attached to the actuator to limit its elongation and control the bending

curvature. With a certain length of cable, the simulation results under pressure of 40 and 80 kPa are shown in Figure 5c. From the results, it can be concluded that under the limitation of cable, the soft origami actuator can increase the bending curvature by increasing the internal air pressure without changing the elongation. By installing a pulley machine with a single servo motor to pull/release cables, the cable length can be controlled. Figure 5d shows the actuator's workspaces with different effective lengths.

3.2. Mechanical Properties of the Scalable Gripper

It has been studied in previous literature that for a specific object, a soft gripper with suitable finger length yields better grasping performance.[7] To this end, we propose a VEL method to increase the contact area based on the size of the objects and thus enlarge the grasping workspace. For example, when grasping a large object, the gripper with a longer length can exert more grasping space to enclose the object than the gripper with a shorter length. In contrast, while grasping a small object, the gripper using a shorter effective length can have more contact area compared with the configuration using a longer length.

ADVANCED
SCIENCE NEWS
www.advancedsciencenews.com

ADVANCED
INTELLIGENT
SYSTEMS
Open Access
www.advintellsyst.com

Figure 5. Validation of origami actuator performance. a) The curvature in the grasping axis versus actuation. b) The maximum blocked force of each finger is 0.45 N in the grasping axis. c) Cable control drive curvature. d) The scalable grip work range.

Here, the effective length is defined as the cable lengths of the scalable gripper. **Figure 6**b shows the vertical forces when actuator length $l_0 = 100$ mm and radius of the circumscribed circle $r = 15$ mm when grasping a spherical object of the same size (60 mm in diameter) with different effective lengths at the same pressure (60 kPa). We set up an experimental platform to test the vertical force of the gripper, as shown in Figure S6, Supporting Information. The red, black, and blue lines represent the force corresponding to the scalable gripper with an effective length of 60, 80, and 100 mm, respectively. And the pull-off force is defined as the maximum force generated during the detaching process. The pull-off forces of the scalable gripper vary with the size of the grasped objects and the effective lengths of the actuator, even if the scalable gripper is inflated with the same pressure.

To test the relationship between pull-off force and the gripped objects' size, which is a function of the VELs, we 3D printed five rigid spheres with different diameters ranging from 10 to 80 mm (Figure 6c). While characterizing the force, we select different effective actuator lengths (40, 60, 80, and 100 mm) for each object. We preset the pressure (60 kPa) and the effective actuator length of the soft gripper according to the parameters we selected. Then, we used the gripper to grasp the five objects to increase the diameter of the spheres. For this experiment, over 20 experimental cases were conducted, and three repeated trials were performed for each case to obtain the mean data.

Figure 6c shows the pull-off force results as a function of the objects' sizes and the effective actuator lengths. We observed that the pull-off forces under the other four lengths exhibit a profile shape of "parabola" which gradually increases to a maximum peak and then decreases as the sphere diameter increases (except the case of VEL = 100 mm). Therefore, there exists an optimal length with the maximum pull-off force for each size of the object. It is noteworthy that the peak values of the five curves appear at different diameters. Specifically, a soft gripper with a longer effective length prefers the spheres' larger diameter and vice versa. For a specific object, the gripper cannot fully conform to the object if the actuator's length is not sufficient. However, if the actuator is too long, the actuator's bending curvature will be smaller than the sphere's curvature, causing grasping failure. Therefore, changing the VELs of the scalable gripper for objects of different sizes can improve grasping performance. We have explored larger grasping area by grasping small size object as shown in Figure S7, Supporting Information; our gripper can grasp objects from 70 to 3 mm.

Another coupled-elongating-and-bending strategy enabled a robotic crawler to embody deployment-combined locomotion (**Figure 7**). We demonstrated the combined crawling motion deployment by designing a contact structure with anisotropic forces with the red end, making it imitate a bioinspired movement pattern based on our approach. The deployable soft crawler
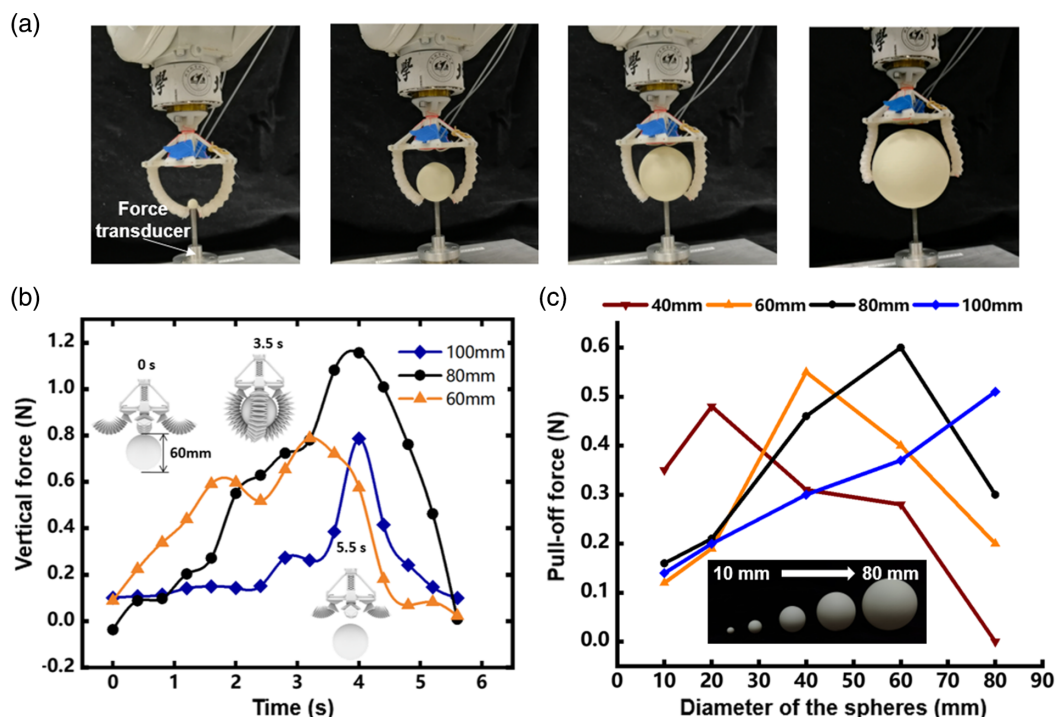
Figure 6. The force results of the gripper under different VEL configurations. a) Measuring the pull-off force of the soft gripper under different effective lengths and different diameter of the sphere. b) Vertical force data of force transduce, when pull the soft gripper with different effective lengths (60, 80, and 100 mm) up and away from the gripped object (60 mm) under pneumatically actuated pressures 60 kPa. c) Pull-off force versus the diameter of the sphere as a function of effective actuator lengths under pneumatically actuated pressures 60 kPa. The inset image shows the spheres with diameters of 10–80 mm.
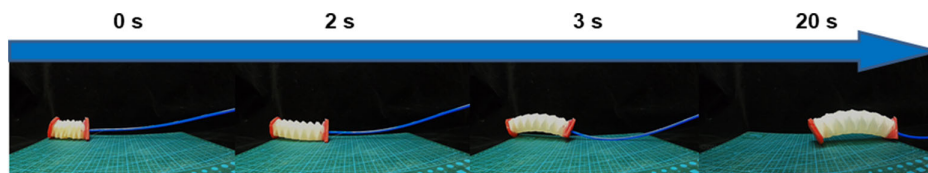
Figure 7. A soft crawling robot, composed of six modules of origami units, demonstrated the deployment of combined crawling motion by designing a contact structure with anisotropic forces with the red end, making it imitate the movement pattern of leeches. For more details, see Video S4, Supporting Information.

could first develop its shape to be ready for locomotion and crawl via repeated inflating and deflating.

4. Conclusion

This study demonstrates a bioinspired origami actuator and combines structural analysis with experimental research on the response of soft origami actuators based on the Yoshimura structure. Compared with the typical Yoshimura structure-based linear actuators and origami tower grippers,[27,28] the soft origami actuators considered in this study can realize the control of motion trajectory and effective length after structural modeling analysis. Guided by the structural and numerical analysis, we designed and built a scalable soft gripper and evaluated its grasping ability for objects of various structures and sizes. More importantly, we found that adjusting the finger's effective length

to the object's size leads to higher gripping power. We also implemented a soft crawling robot composed of six modules of origami units.[29]

The manufacturing process needs improvement in the future. Although the complex inner cavity can be manufactured by lost wax casting, it is exceedingly time-consuming and error prone. We also used an Objet Connex500 C3 3D printer (Stratasys Ltd., Eden Prairie, MN, USA) to directly fabricate the origami architectures; the material is Agilus30 (Young's modulus 0.66 MPa). Although 3D printing enabled direct printing of complex origami structures, it has several drawbacks, such as limited material availability, high price, and difficulty in mass production. Furthermore, the elongation ratio of Agilus30 was much lower than that of highly stretchable elastomers used in the lost wax casting method (elongation limit, ≈1000%), resulting in poor repeatability and robustness.

In this study, our design only includes the bending and elongation in two-dimensions. Future prototypes could also incorporate 3D (out of plane) bending and elongation, material stiffness variability, or the incorporation of reinforcing fibrous components for added functionality.[30] In addition, by optimizing the origami structure's size and shape, the actuator's overall grasping performance can be improved.

Supporting Information

Supporting Information is available from the Wiley Online Library or from the author.

Conflict of Interest

The authors declare no conflict of interest.

Data Availability Statement

Research Data is not shared.

[1] Y. Wang, X. Yang, Y. Chen, D. K. Wainwright, C. P. Kenaley, Z. Gong, Z. Liu, H. Liu, J. Guan, T. Wang, J.C. Weaver, *Sci. Robot.* **2017**, *2*, 1.
[2] H. Feng, N. Chai, W. Dong, *PLoS One* **2015**, *10*, 1.
[3] S. Li, Y. Zhang, X. Dou, P. Zuo, J. Liu, *J. Mech. Behav. Biomed. Mater.* **2018**, *86*, 345.
[4] J. Lim, H. Park, J. An, Y. S. Hong, B. Kim, B. J. Yi, *Mechatronics* **2008**, *18*, 315.
[5] J. D. Greer, L. H. Blumenschein, A. M. Okamura, E. W. Hawkes, *Proc. – IEEE Int. Conf. Robot. Autom.* **2018**, *2*, 4165.
[6] Z. Xie, F. Yuan, Z. Liu, Z. Sun, E. M. Knubben, L. Wen, *IEEE/ASME Trans. Mechatron.* **2020**, *25*, 1841.
[7] Y. Hao, Z. Liu, J. Liu, X. Fang, B. Fang, N. Shilin, Y. Guan, F. Sun, T. Wang, L. Wen, *Smart Mater. Struct.* **2020**, *29*, 3.
[8] W. Kim, J. Byun, J. K. Kim, W. Y. Choi, K. Jakobsen, J. Jakobsen, D. Y. Lee, K. J. Cho, *Sci. Robotics* **2019**, *4*, eaay3493.
[9] H. Jiang, X. Liu, X. Chen, Z. Wang, Y. Jin, X. Chen, in *ROBIO*, IEEE, Qingdao, China, December 3–7 **2016**, pp. 350–356.
[10] M. Manti, T. Hassan, G. Passetti, N. D'Elia, C. Laschi, M. Cianchetti, *Soft Robot.* **2015**, *2*, 107.
[11] J. M. Gattas, Z. You, *Eng. Struct.* **2015**, *94*, 149.
[12] Y. Yoshimura, National Advisory Committee on Aeronautics (NACA), TM1390 **1955**.
[13] C. D. Onal, R. J. Wood, D. Rus, *IEEE/ASME Trans. Mechatron.* **2013**, *18*, 430.
[14] M. Salerno, K. Zhang, A. Menciassi, J. S. Dai, *Proc. – IEEE Int. Conf. Robot. Autom.* **2014**, 2844.
[15] H. Matsuo, H. H. Asada, Y. Takeda, *IEEE Robot. Autom. Lett.* **2020**, *5*, 2730.
[16] Z. Gong, X. Fang, X. Chen, J. Cheng, Z. Xie, J. Liu, B. Chen, H. Yang, S. Kong, Y. Hao, T. Wang, J. Yu, L. Wen, *Int. J. Rob. Res.* **2020**, *40*, 449.
[17] T. Hainsworth, L. Smith, S. Alexander, R. MacCurdy, *IEEE Robot. Autom. Lett.* **2020**, *5*, 4118.
[18] B. S. Homberg, R. K. Katzschmann, M. R. Dogar, D. Rus, *Auton. Robots* **2019**, *43*, 681.
[19] R. L. Truby, M. Wehner, A. K. Grosskopf, D. M. Vogt, S. G. Uzel, R. J. Wood, J. A. Lewis, *Adv. Mater.* **2018**, *30*, 1706383.
[20] B. Shih, D. Drotman, C. Christianson, Z. Huo, R. White, H. I. Christensen, M. T. Tolley, in *IROS*, IEEE, Vancouver, Canada, September 24–28 **2017**, pp. 494–501.
[21] M. A. Roa, R. Suarez, *IEEE Trans. Robot.* **2009**, *25*, 839.
[22] H. Jiang, E. W. Hawkes, C. Fuller, M. A. Estrada, M. R. Cutkosky, *Sci. Robot.* **2017**, *2*, eaan4545.
[23] K. Lee, Y. Wang, C. Zheng, *IEEE Trans. Robot.* **2020**, *36*, 488.
[24] R. V. Martinez, C. R. Fish, X. Chen, G. M. Whitesides, *Adv. Funct. Mater.* **2012**, *22*, 1376.
[25] L. Paez, G. Agarwal, J. Paik, *Soft Robot.* **2016**, *3*, 109.
[26] S. Abondance, C. B. Teeple, R. J. Wood, *IEEE Robot. Autom. Lett* **2020**, *5*, 5502.
[27] J. Cai, X. Deng, Y. Xu, J. Feng, *J. Mech. Robot.* **2016**, *8*, 021017.
[28] E. Vander Hoff, D. Jeong, K. Lee, *IEEE Int. Conf. Intell. Robot. Syst.* Chicago, IL, USA, September 14–18 **2014**, pp. 1421–1426.
[29] W. Kim, J. Byun, J. K. Kim, W. Y. Choi, K. Jakobsen, J. Jakobsen, D. Y. Lee, K. J. Cho, *Sci. Robot.* **2019**, *4*, 1.
[30] L. Wen, F. Pan, X. Ding, *Sci. Robot.* **2020**, *5*, 3.